Temperature dependence of the photoreflectance spectra of a GaAs/$Al_{0.3}Ga_{0.7}As$ doping superlattice

Ulrich D. Keil,* Norbert Linder, Klaus Schmidt, and Gottfried H. Döhler
Institut für Technische Physik, Universität Erlangen-Nürnberg, D8520 Erlangen, Federal Republic of Germany

Jeff N. Miller
HP-Laboratories, Palo Alto, California 94803
(Received 9 April 1991)

The optical properties of a GaAs/$Al_{0.3}Ga_{0.7}As$ hetero-*n-i-p-i* crystal with GaAs quantum wells in the intrinsic region ("type II") have been investigated by photoreflectance measurements. To understand the complex spectra we have varied several measurement parameters such as ac pump intensity, dc pump intensity, pump frequency, and temperature. The latter one represents a very useful tool to vary the degree of excitation of the sample over a wide range while keeping the pump and probe light intensities at a constant level. The role of temperature is described by a simple model which takes into account the strong temperature dependence of the thermally activated recombination kinetics. The photoreflectance spectra are compared with spectra calculated within the framework of a semiclassical Franz-Keldysh model and a model considering an infinite quantum well in an electric field (quantum-confined Franz-Keldysh model). From this comparison the internal electric field can be deduced. We demonstrate that it is essential to take into account the fact that the dielectric function has a spatial dependence with the period of the superlattice.

I. INTRODUCTION

n-i-p-i structures are very sensitive to optical excitation, as the electrons and holes are spatially separated by the built-in electric fields. It has been expected[1] and recently demonstrated[2,3] that *n-i-p-i* doping superlattices exhibit strong optical nonlinearities due to changes of the internal fields under optical excitation. This results in a shift of the band gap, the subband energies, and a change in the overlap of the electron and hole wave functions in the case of short periods. In the case of long periods a semiclassical picture applies and the change of absorption is suitably described as an internal Franz-Keldysh effect. The change of absorption is related to a change in the refractive index Δn by the Kramers-Kronig relation. Therefore *n-i-p-i* crystals are particularly suitable for photoreflectance (PR) measurements and have recently been studied by this technique.[4–7]

Although these experiments have fully confirmed the above-mentioned theoretical expectations, it seems appealing not only to observe these more semiclassical phenomena but also the typical quantum properties associated with the formation of two-dimensional subbands in PR experiments. Two-dimensional subbands in conventional *n-i-p-i* structures have been demonstrated clearly by resonant Raman scattering[8] or magnetoconductivity[9] studies. Experiments involving the transitions between conduction and valence bands, such as luminescence or PR studies, have not, or at least only marginally, been successful. This observation can be understood if one considers the effect of the potential fluctuations in *n-i-p-i* structures due to the random distribution of impurities in the doping layers. The effect of these potential fluctuations on the energies of different subbands is more or less correlated, which results in a reduction of the spatial fluctuations observed as a broadening in intersubband transitions. The potential fluctuations of different doping layers are, however, nearly uncorrelated and, therefore, lead to a stronger broadening of luminescence and absorption spectra. Moreover, even relatively steep exponential tails of the subband density of states can completely obscure the effect due to transitions between different subbands, as transitions probabilities involving lower subbands are exponentially smaller as well.

An elegant solution to overcome this disadvantage of the *n-i-p-i* structure and still preserve its attractive properties is provided by the "type-II" hetero-*n-i-p-i* structure,[10] which is the subject of the present study. As shown in Fig. 1 these superlattices are composed of two different semiconductors with different band gaps. Compared to a homo-*n-i-p-i* structure, the type-II hetero-*n-i-p-i* structure exhibits more pronounced subband effects due to the additional confinement of the charge carriers in the (triangular) quantum wells (QW's) and because of the spatial separation between the free carriers and the ionized impurities. The latter reduces the potential fluctuations which broaden the subbands in homo-*n-i-p-i* crystals.

Concerning optical effects, type-II hetero-*n-i-p-i* structures should behave similarly to a multiple quantum well in an external field as investigated by Miller *et al.*[11,12] In our case, however, the absorption of photons and the generation of charge carriers change the internal electric field. The photoexcited charge carriers are separated by

the internal field and, therefore, the recombination probability is small. This leads to an effective change of the electric field related to a change in absorption even for low light intensities.

As the well width of our sample was 300 Å, we are in the limit to observe Franz-Keldysh oscillations (FKO) as well as subband effects. The transition from the quantum-confined Franz-Keldysh (QCFK) effect to the semiclassical Franz-Keldysh (FK) effect has been discussed by Miller *et al.* for a QW in a uniform electric field[11] and by Döhler *et al.* for *n-i-p-i* structures.[10]

We compare the spectra that we have measured with spectra calculated with the semiclassical FK model and the quantum-mechanical QCFK model. In the latter calculations the type-II sample is treated as an infinitely high QW in an electric field. In this model we neglect excitonic effects and band-filling effects. Also we do not take into account the self-consistent changes of the potential due to photoinduced charges and the interactions of light- and heavy-hole states. Recent self-consistent calculations by Forkel[13] using a realistic band structure with heavy- and light-hole mixing show a shift of the transition energies of about 10 meV to lower energies compared to the simple model. But as the electronic structure and excitation level of the sample depend on several parameters, such as doping concentration, thickness, and lifetime of the charge carriers which are not exactly known, the simple model is good enough to demonstrate qualitatively the behavior of the structure.

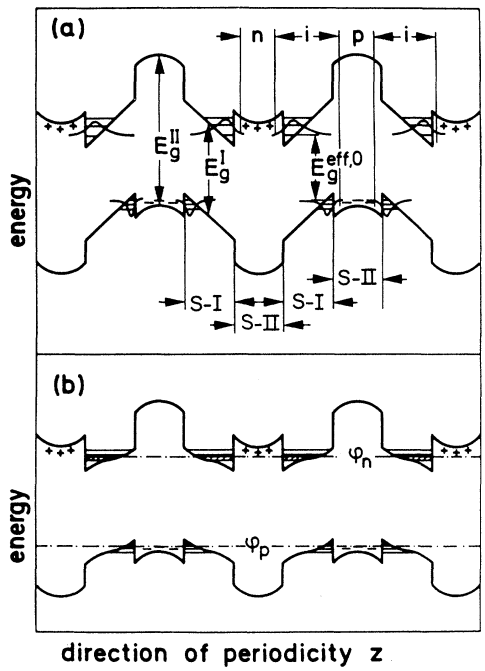

FIG. 1. Band diagrams for a type-II hetero-*n-i-p-i* structure in ground state and excited state. *S*-I denotes the semiconductor with the smaller band gap E_g^{I} and *S*-II the large band gap (E_g^{II}) semiconductor. The nominal parameters of the investigated sample are $d_{GaAs} = 300$ Å, $d_n = 50$ Å, $d_{in} = 50$ Å, $d_p = 50$ Å, $d_{ip} = 25$ Å, $n_D = 3 \times 10^{18}$ cm^{-3}, $n_A = 3 \times 10^{18}$ cm^{-3}, $F_0 = 1.04 \times 10^5$ V/cm, $d_{nom} = 850$ Å.

The spatial dependence of the change of the dielectric function $\Delta\epsilon(z)$ in the z direction perpendicular to the layers represents another property which influences PR spectra of *n-i-p-i* structures. This effect is important as the period d of a *n-i-p-i* crystal is not small compared to the wavelength λ/n_{opt}. This becomes evident in our investigations of GaAs *n-i-p-i* structures.[14]

With another model we simulate the dependence on temperature, pump intensity, and pump frequency. In this classical model thermally activated vertical recombinations are considered in order to explain qualitatively the variations of the recombination lifetime of the charge carriers in the QW's. The recombination probability is significantly higher for higher temperature. So this model is able to explain how temperature variations can be used to tune the charge carrier density over a wide range. This is important in our case as the sample had no electric contacts for adjusting the charge carrier density.

II. EXPERIMENT

The sample was grown on an undoped GaAs substrate by molecular-beam epitaxy (MBE). It consists of ten periods beginning and ending with a *p*-type doped $Al_{0.3}Ga_{0.7}As$ layer. The band profiles are shown for one period in Fig. 1. The nominal design parameters are given in the figure caption. The actual sample parameters differ from these nominal parameters depending on the position on the wafer as the sample was not rotated during MBE growth.

The experimental setup was a conventional PR setup with a He-Ne laser as the pump beam source and a monochromator with a tungsten lamp as the probe beam source. The sample exhibits strong luminescence, which cannot be distinguished easily from the change of reflection by phase sensitive measurement methods. Although the luminescence is independent of the probe beam wavelength and can be subtracted after the measurement, this background reduces the sensitivity for the change of reflection. Three different approaches were used to increase the ratio $\Delta R\, I_0/I_{lum}$ (I_0 is the probe beam intensity, typically $I_0 = 5$ μW/cm^2; I_{lum} is the luminescence intensity).

(i) Measuring the second harmonic of the signal suppresses the luminescence because the luminescence signal exhibits a much shorter time constant and is therefore mainly seen in odd harmonics of the pump frequency. The disadvantage is that the signal degrades, which implies that this method could not be used for small modulation amplitudes which, on the other hand, are required in order to achieve a high resolution of subband structures.

(ii) Measuring under an incidence angle of the probe beam of about 50° was only possible outside of our cryostat setup. In this case the probe beam was defocused on the sample and focused onto a pinhole between sample and detector in order to minimize the detection of luminescence light. This procedure, however, could not be applied with our cryostat setup.

(iii) By spatially separating the pump and the probe beam by about 5 mm we increased the ratio $\Delta R I_0/I_{\rm lum}$ from 0.1 to 4. This was possible because of the long lifetime of the photoinduced charge carriers compared to the anomalously fast diffusion time, which is shorter than 50 μs.[15] So the charge carriers are distributed over the whole sample before they recombine. This will be discussed in more detail below.

Calculations by Metzner[16] have shown that we have a highly excited region at the pump beam spot (about 0.5 mm diameter in our case) with a high recombination probability and strong luminescence, if the pump intensity is high. The charge carriers that leave the excitation area by diffusion are distributed over the rest of the sample (sample area is 1.25 cm^2 in our case) resulting in a relatively low excitation and long charge carrier lifetimes outside the pump beam spot. In contrast to a setup with an attenuated pump beam at the probe beam spot, laser intensity fluctuations are leveled out as the recombination probability is higher for high excitation. The charge carrier density almost saturates in this region leading to a stable excitation level. By this means it is possible to measure reflectivity changes for small excitation changes with an increased ratio $\Delta R I_0/I_{\rm lum}$.

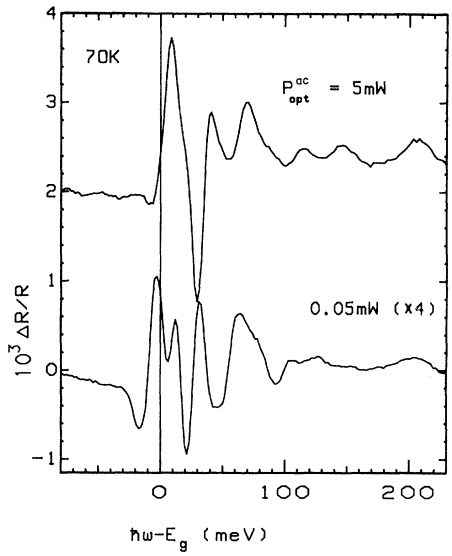

FIG. 3. PR spectra for different ac pump power at 70 K (spectrum for $P^{ac}_{opt} = 5$ mW shifted). $P^{ac}_{opt} = 5$ and 0.05 mW corresponds to an intensity $I^{ac}_{pump} < 4$ and 0.04 mW/cm^2, respectively.

III. EXPERIMENTAL RESULTS

PR spectra of our sample for different temperatures are shown in Fig. 2. The redshift of the band gap with increasing temperature is eliminated in this figure by using $\hbar\omega - E_g(T)$ as the abscissa. We have used the values $E_g(T)$ given in Landolt-Börnstein[17] for the temperature-dependent band gap. For high temperature the spectra resemble those of FKO's. For lower temperatures subband effects become evident. The transitions broaden for high temperatures and the subband structures cannot be resolved. The temperature dependence of the broadening can be explained by electron–LO-phonon interactions as their number increases for higher temperature.[18] In addition to this broadening we expect a temperature-independent broadening, as the periods are not exactly equal and the inhomogenous excitation due to absorption

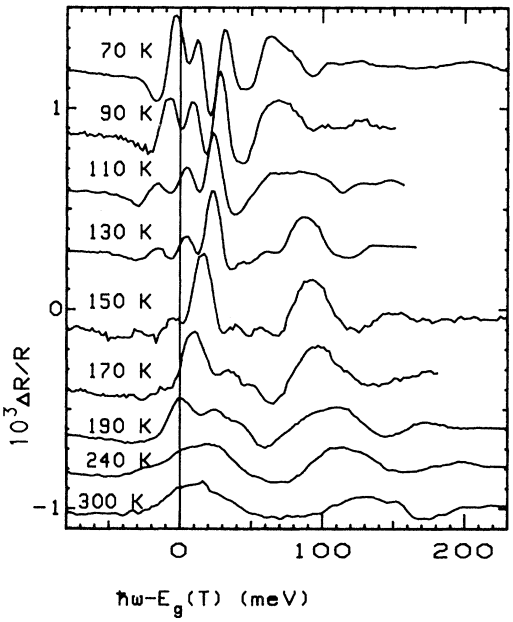

FIG. 2. Photoreflectance spectra at different temperatures with an ac pump power $P^{ac}_{opt} = 5$ mW (to distinguish the spectra different offsets are added).

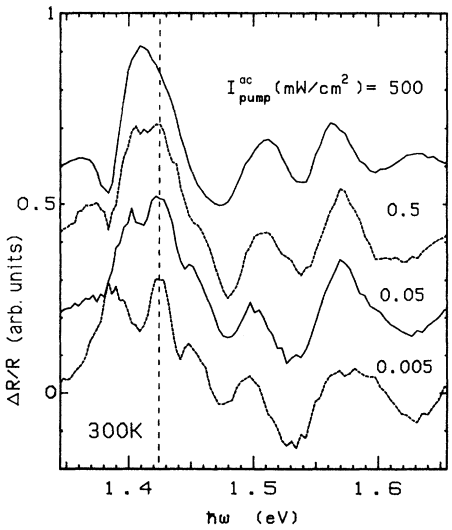

FIG. 4. PR spectra for different ac pump power at 300 K (setup different from the measurement at 70 K).

of the pump light leads to different degrees of excitations in the different QW's.

With increasing temperature the period of the FKO's becomes longer and the subband structures shift to lower energies, both indicating a higher field and a smaller indirect band gap in real space. We explain the redshift of the subbands as an effect of the reduced carrier lifetime at higher temperatures, resulting in a lower excitation for the same light intensity. This is related to a higher field as there are fewer photoinduced charge carriers compensating the space charge of the donors and acceptors. In addition to the shift of the subbands the lower field leads to a shorter period of the FKO's which depend on the electric field as $E^{-2/3}$.[19–21]

In contrast to the strong shifts caused by temperature variations, a reduction of the ac pump intensity leads to a weak redshift of the subband structure (Fig. 3). In addition to the shift a higher resolution is observed for the small modulation amplitude. The pump intensity is estimated by assuming that the photoexcited charge carriers spread homogeneously over the whole sample. We find an upper limit for the optical pump intensity of $I^{ac}_{pump} = 4$ mW/cm^2 for $P^{ac}_{opt} = 5$ mW.

In a more sensitive setup outside the cryostat with an incidence angle of 50° as described in Sec. II and a wider range of optical excitation intensities with pump and probe beam on the same spot we were able to observe subband effects even at 300 K. In this case we could also see a redshift of the subband structure with decreasing pump beam intensity (Fig. 4).

By applying an additional dc pump beam at 70 K we observed only a very weak shift of the spectra, which practically disappeared at a ratio $I_{dc}/I_{ac} = 0.2$. We also changed the pump frequency (Fig. 5). The spectra shift

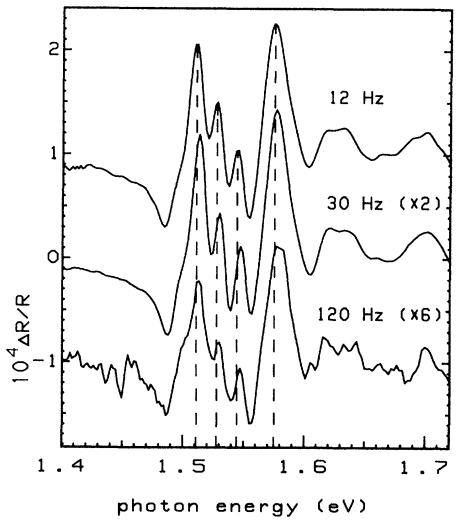

FIG. 5. Dependence of PR spectra on pump frequency (an offset is added to the spectra). The positions of the peaks for 12 Hz are marked by dashed lines. The spectra for 30 and 120 Hz are multiplied by a factor of 2 and 6, respectively.

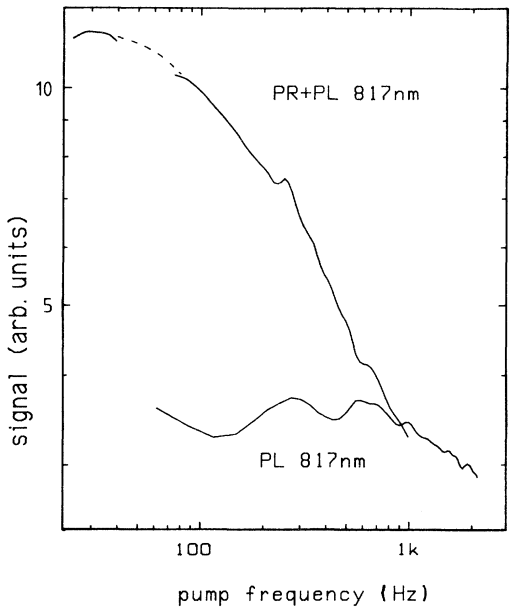

FIG. 6. Dependence of PR intensity $\Delta R I_0$ (PR) and luminescence intensity I_{lum} (PL) on pump frequency for a fixed wavelength. The frequency range around 50 Hz could not be measured due to a high noise level at the main frequency.

to higher energies for higher frequencies. At higher pump frequencies not all the charge carriers can recombine fast enough and the sample does not relax into the ground state. This yields a higher average excitation. The "lifetime" of the charge carriers was measured by tuning the pump frequency and detecting the PR signal at a fixed wavelength of 817 nm. At 70 K we can estimate lifetimes to be of the order of 10 ms (Fig. 6). At this point it should be pointed out that the lifetime depends on the excitation level and increases strongly for decreasing excitation (and, therefore, higher internal electric fields). Thus the dynamic behavior cannot be described by a single lifetime. In particular, the time constant for reaching the steady state during excitation (pump on) is much shorter than the time for returning to the ground state (pump off).

IV. DISCUSSION AND COMPARISON WITH THEORY

A. Spatial dependence of the dielectric function

For a comparison of the measured spectra with calculations we have to consider the spatial dependence of the change of the dielectric function $\Delta\epsilon$, which is due to the periodic variation of the material composition and the electric-field changes. We actually observe an effective change $\langle\Delta\epsilon\rangle_{eff}$ (Ref. 21)

$$\langle\Delta\epsilon(\omega)\rangle_{\text{eff}} = 2ik\int_0^{md}\Delta\epsilon(\omega,z)e^{2ikz}\,dz\,, \tag{1}$$

with wave number $k = 2\pi n_{\text{opt}}(\lambda)/\lambda$ in a sample with m n-i-p-i periods. In the following we assume that $\Delta\epsilon(F;\Delta F)$ is constant within the GaAs region and $\Delta\epsilon=0$ in the AlGaAs region. If the excitation level is uniform for all the n-i-p-i periods for photon energies well below the AlGaAs band gap, this yields

$$\langle\Delta\epsilon\rangle_{\text{eff}} = \Delta\epsilon(F,\Delta F)(e^{2ik(d_i+d_p+d_{ip})} - e^{2ik(d_p+d_{ip})} + e^{2ik(d-d_{ip})} - e^{2ik(d-d_{ip}-d_i)}) \times\sum_{\nu=1}^{m} e^{2ik\nu d}\,, \tag{2}$$

which can be written as

$$\langle\Delta\epsilon\rangle_{\text{eff}} = (\alpha^* + i\beta^*)(\Delta\epsilon_1 + i\Delta\epsilon_2) \tag{3}$$

with the factors α^* and β^* describing the contributions of $\Delta\epsilon_1$ and $\Delta\epsilon_2$ to the real and imaginary part of the effective change of the dielectric constant $\langle\Delta\epsilon\rangle_1$ and $\langle\Delta\epsilon\rangle_2$ (a calculated example is shown at the bottom of Fig. 10). In Eq. (2) the factors in parentheses take into account the phase shift of the light in one n-i-p-i period and the sum describes the multiple beam interference with contributions from all the periods. This results in a periodic change between real and imaginary parts $\Delta\epsilon_1$ and $\Delta\epsilon_2$, respectively, contributing to $\Delta R/R$ spectra, which are calculated by

$$\frac{\Delta R}{R} = \alpha\langle\Delta\epsilon\rangle_1 + \beta\langle\Delta\epsilon\rangle_2, \tag{4}$$

with the Seraphin coefficients α and β.[23]

B. FK model

At first the semiclassical FK model was used to calculate PR spectra. A comparison of the calculated spectra with the measured data shows that it is essential to take into account the spatial dependence of $\Delta\epsilon$. Figure 7 shows results of calculations for different period length d (denoted by the ratio d/d_{nom}, where d_{nom} is the nominal thickness of 850 Å) compared to a PR spectrum measured at 300 K. The spectra change evidently by varying the parameter d. The best fit is obtained for $d/d_{\text{nom}} = 0.94$ and an electric field $F_0 = 1\times10^5$ V/cm in the ground state and a field modulation $\Delta F = 3\times10^3$ V/cm. In this case even the lower amplitude of the maximum at 1.68 eV is reproduced correctly. It should be pointed out that the calculated and experimental spectra are shown on the same scale. Therefore a comparison between the calculated and measured amplitudes provides information about the value of ΔF. In these calculations a two-band model was used with effective electron and hole masses of $m_c = 0.067$ and $m_v = 1/\gamma_1 = 0.146$,[17] respectively, and an interband matrix element of $E_p = 2P^2/m_0 = 28.9$ eV.[23]

Figure 8 shows PR spectra calculated with $d/d_{\text{nom}} = 0.94$ for different fields in the ground state F_0. By comparing with the measured spectra in Fig. 2 we deduce the relation between temperature and internal electric fields as given in Table I.

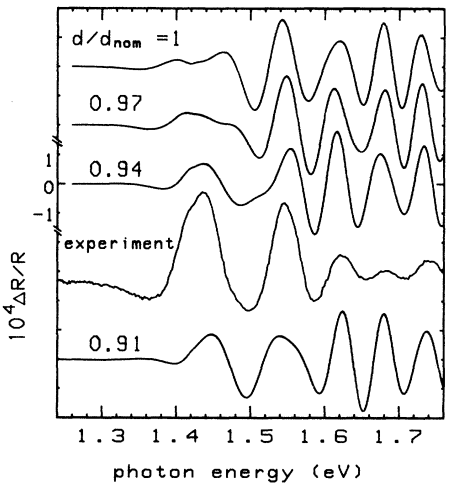

FIG. 7. PR spectra calculated in the FK model with the spatial dependence of $\Delta\epsilon$ included. The spectra are calculated with a maximum electric field $F_0 = 1\times10^5$ V/cm and $\Delta F = 3\times10^3$ V/cm for different period lengths d, denoted by the ratio d/d_{nom}. In addition, a PR spectrum measured at 300 K is shown.

Because the PR spectra, especially for low temperature, do not exhibit pure FKO, it is not possible to calculate the internal field by the evaluation of the oscillation period. In addition, the spatially periodic change of

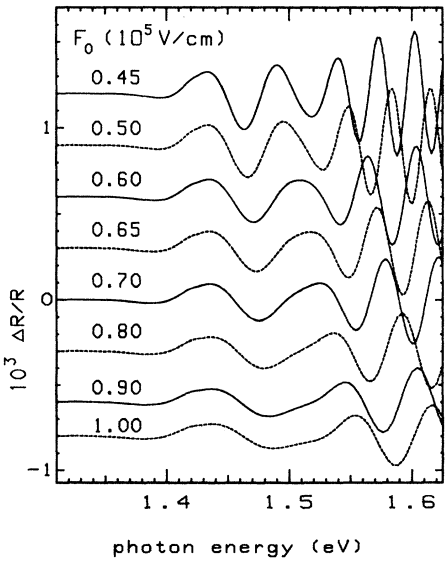

FIG. 8. PR spectra calculated in the FK model with $d/d_{\text{nom}} = 0.94$ for different electric fields F_0 and $\Delta F = 3\times10^3$ V/cm.

TABLE I. Electric-field values and broadening parameter Γ for different temperatures deduced by comparison with the FK model and the QCFK model.

	FK model	QCFK model	
T (K)	F_0 (10^5 V/cm)	F_0 (10^5 V/cm)	Γ (meV)
70	0.45	0.45	5
90	0.50	0.50	5
110	0.60	0.60	6
130	0.65	0.61	6
150	0.68	0.70	7
170	0.72	0.79	8
190	0.80	0.94	10
240	0.90	0.97	17
300	1.00	1.00	24

the dielectric function in this case indicates a higher electric field than is actually present, as the first oscillation period is stretched.

The FK model gives a first estimation of the internal field. In the following we demonstrate that these values are consistent with calculations of $\Delta R/R$ spectra in the QCFK model.

C. QCFK model

Figure 9 shows the calculated $\Delta R/R$ spectra for an infinite QW in different electric fields to be compared with the measured spectra in Fig. 2 for different temperatures. As the spectra are rather complex, Fig. 10 explains the contributions of the interference effects (α^*, β^*) and the subband transitions that take part in the spectrum for a

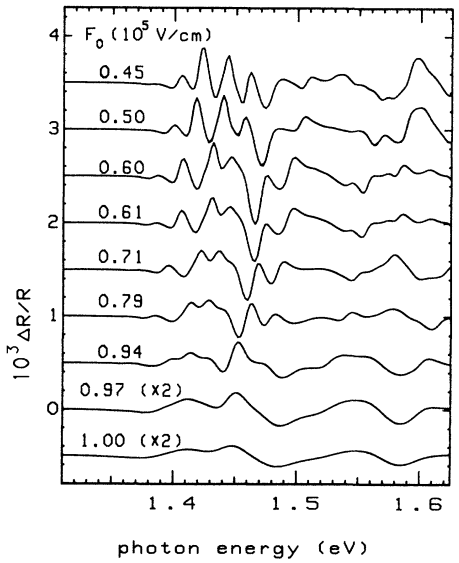

FIG. 9. PR spectra calculated in the QCFK model with $d/d_{\rm nom}$ =0.94 for different electric fields F_0 and $\Delta F = 3\times10^3$ V/cm. The used broadening parameters Γ are given in Table I.

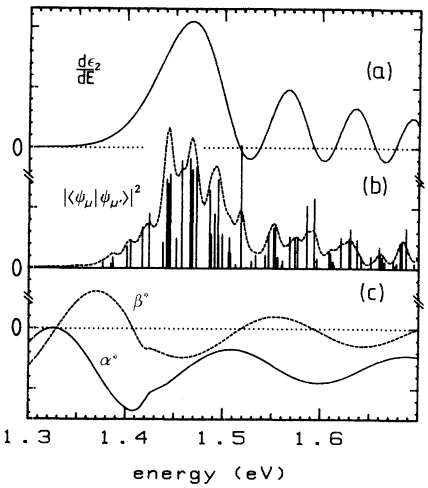

FIG. 10. (a) Derivative of ϵ_2 calculated in the FK model; (b) derivative of ϵ_2 in the QCFK model (dashed line) with Γ = 4 meV and overlap of electron and hole wave functions contributing to the calculated spectra; (c) factors α^* and β^* (dashed line) describing the effect of the spatially periodic $\Delta\epsilon$ calculated with $F = 1\times10^5$ V/cm, $d/d_{\rm nom}$ = 0.94, and $d_{\rm GaAs}$ = 282 Å (all in arbitrary units).

field $F = 1\times10^5$ V/cm with the height of the lines proportional to the overlap integral $|\langle\Psi_{\mu,c}|\Psi_{\mu',vi}\rangle|^2$. This is compared to the derivative of $\Delta\epsilon_2$, calculated in the FK picture, which is roughly seen as an envelope of the overlaps. There are a lot of transitions that determine the calculated spectra, because there are no selection rules for the quantum numbers μ and μ' of the electron and hole states. In contrast to the FK model, this model takes into account light- and heavy-hole contributions with m_{vh} = 0.4 and m_{vl} = 0.074 and the interband matrix element P^2 (heavy hole) and $P^2/3$ (light hole).

Figure 10 also shows that it is not possible to correlate a single transition to structures in the measured PR spectra. Only groups of transitions can be resolved.

Again the influence of the spatially periodic $\Delta\epsilon$ on the spectra is strong. The thickness d used in the calculations determines which structures in the spectra are emphasized [Fig. 10 and Eq. (3)]. As before, the best agreement with the experiments is found for d 6% smaller than $d_{\rm nom}$.

As discussed in the Introduction, the QCFK model is a rather crude model compared to the complex situation in a hetero-*n*-*i*-*p*-*i*-structure. It does not take into account excitonic effects, band-filling effects, band bending, and a realistic band structure. So this model is not good enough to reproduce the measured spectra, but the shifts of the spectra depend very sensitively on the change of the fields and the shifts can provide information about the relative field variations. Starting from the field values obtained from the FK model for high temperatures, which could be determined very accurately, we deduce a modified relation between the temperature and electric

field in the QW's as given in the third column of Table I. The uncertainty of the determined field caused by this comparison is smaller than 1×10^3 V/cm.

The temperature-dependent broadening of the step functions occurring in the imaginary part of the dielectric function at the D_0 critical points has been taken into account by substituting[24]

$$\Theta(x) \rightarrow \frac{1}{2} + \frac{1}{\pi} \arctan(x) , \tag{5}$$

where

$$x = \frac{\hbar\omega - E_{\mu,\mu'}}{\Gamma} , \tag{6}$$

with the individual intersubband gaps $E_{\mu,\mu'}$ and the broadening parameter Γ. The used broadening parameters are given in Table I. The results of our calculations with $F_0 = 1 \times 10^5$ V/cm and $\Gamma = 24$ meV (corresponding to our 300-K experiments) demonstrate quite well the transition regime from the semiclassical FK model to the quantum-mechanical QCFK model for PR spectra. The amplitude is higher in the FK model as in this case no broadening was regarded. In Fig. 11 calculations for both models are compared with the experiment. In both cases very good agreement is obtained for $d/d_{\text{nom}} = 0.94$.

Finally, it should be pointed out that although the effect of the periodic change of real and imaginary part of the dielectric function contributing to $\Delta R/R$ complicates the interpretation of the spectra, it would be very interesting to design a sample in a way that the principal peak of the multiple beam interference is near the band gap. This is equivalent to a tunable Bragg reflector as discussed by Linder and Döhler[25] and can increase the ratio $\Delta R/R$ by a factor of 100.

D. Thermally activated vertical recombination

The important question of why the spectra depend so strongly on temperature but only weakly on pump intensity and frequency still needs to be answered. In order to understand this observation we simulate the excitation recombination kinetics with the simple classical model depicted in Fig. 12. The electrons have to be thermally activated over the barrier $\Delta V(n^{(2)})$ in order to recombine with the holes if tunneling through the triangular barrier is neglected. The barrier height $\Delta V(n^{(2)})$ depends linearly on the two-dimensional density $n^{(2)}$ of optically induced charge carriers

$$\Delta V(n^{(2)}) = \frac{e^2}{\epsilon\epsilon_0} \left(n_D \frac{d_n}{2} - n^{(2)} \right) d_i . \tag{7}$$

The recombination lifetime for thermally activated transitions is given by

$$\tau = \tau_0 \exp\left(\frac{\Delta V(n^{(2)})}{kT} \right) . \tag{8}$$

Using Eqs. (7) and (8) we obtain for the change of the sheet charge carrier density

$$\dot{n}^{(2)} = -\dot{n}^{(2)}_{\text{rec}} + \dot{n}_{\text{opt}} d \tag{9}$$

$$= -\frac{n^{(2)}}{\tau_0} \exp\left(-\frac{\frac{e^2}{\epsilon\epsilon_0} \left(n_D \frac{d_n}{2} - n^{(2)} \right) d_i}{kT} \right) + \dot{n}_{\text{opt}} d . \tag{10}$$

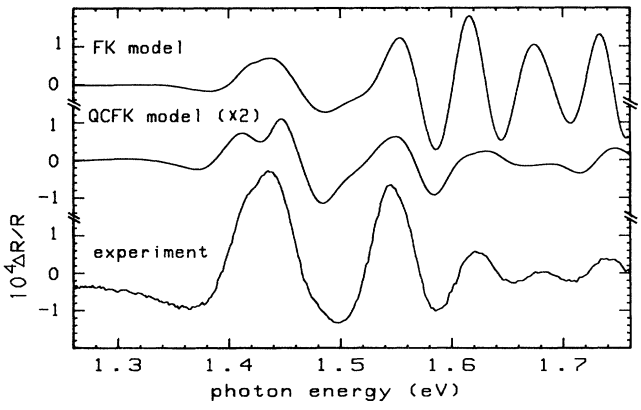

FIG. 11. Comparison of calculations in the FK model and the QCFK model with a PR spectrum measured at 300 K. The parameters used in the calculations are $F_0 = 1 \times 10^5$ V/cm, $\Delta F = 3 \times 10^3$ V/cm, $d/d_{\text{nom}} = 0.94$, and for the QCFK model $\Gamma = 24$ meV.

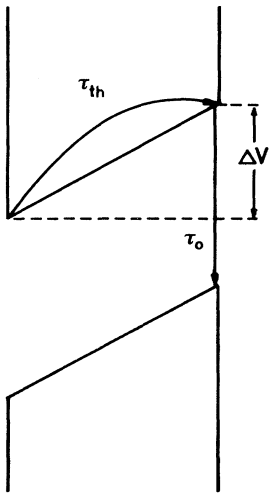

FIG. 12. Model: thermally activated vertical recombination.

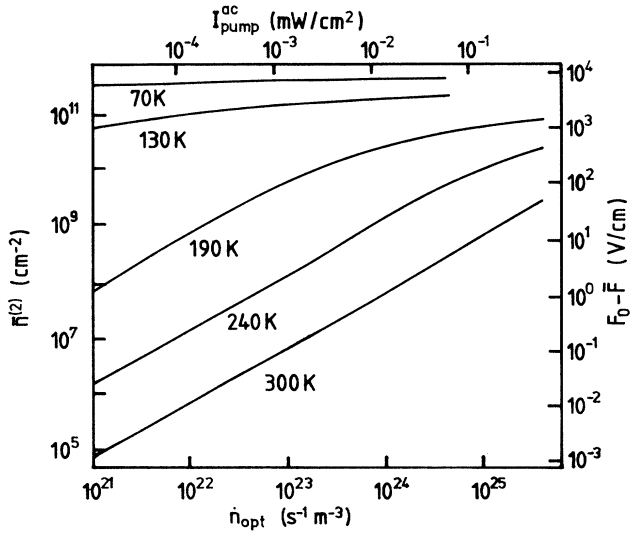

FIG. 13. Calculated dependence of the averaged charge carrier density $\bar{n}^{(2)}$ on the intensity of optical excitation $\dot{n}_{opt}$ for different temperatures and a pump frequency of 10 Hz. The right scale shows the related averaged internal electric field. The upper scale shows the light intensity I^{ac}_{pump} calculated from the absorbed photons per time.

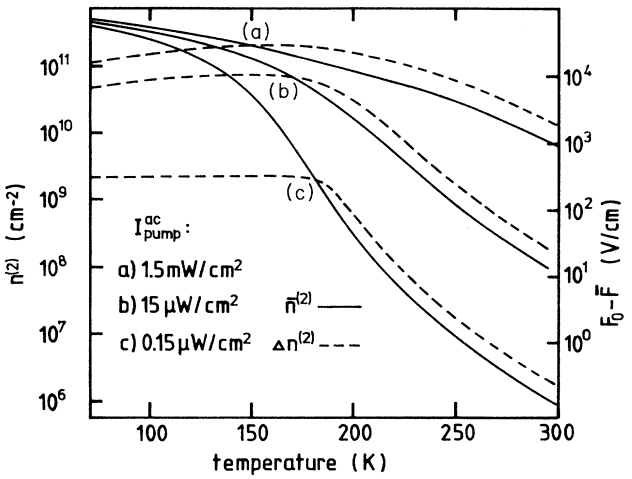

FIG. 14. Calculated dependence of $\bar{n}^{(2)}$ and $\Delta n^{(2)}$ on the temperature for different I^{ac}_{pump} and a pump frequency of 10 Hz.

For the recombination time in the QW at zero field we use $\tau_0 = 3$ ns.[26] For a typical excitation intensity of 1 mW/cm², a photon energy of 1.96 eV (HeNe laser), and an average absorption coefficient for $GaAs/Al_{0.3}Ga_{0.7}As$ of 20 000 cm^{-1} (Ref. 27), we calculate an electron-hole generation rate of 6×10^{18} $cm^{-3}s^{-1}$. With this value we have related the upper scale (I^{ac}_{pump}) with $\dot{n}_{opt}$ in the following graph.

Figure 13 shows the dependence of the photogenerated sheet carrier density $n^{(2)}$ on the optical excitation intensity I^{ac}_{pump} for different temperatures. The charge carrier density averaged over the time $\bar{n}^{(2)}$ changes only by about 20% for 70 K even if I^{ac}_{pump} is changed over four orders of magnitude. Changing the temperature, however, influences $\bar{n}^{(2)}$ drastically. $\bar{n}^{(2)}$ is related to the averaged internal electric field $\bar{F}$ shown on the scale to the right of the graph. As $\bar{F}$ determines the PR spectra this explains why they are not strongly affected by a change of I^{ac}_{pump}. Another parameter that determines mainly the amplitude of the spectra is the change of carrier density and field $\Delta n^{(2)}$ and ΔF, respectively. Figure 14 shows the dependence of $\bar{n}^{(2)}$ and $\Delta n^{(2)}$ on the temperature for different pump intensities I^{ac}_{pump}, again indicating a strong temperature dependence for both of them.

V. SUMMARY

We have investigated the influence of temperature, dc and ac pump intensity, and pump frequency on PR spectra of type-II hetero-*n*-*i*-*p*-*i* structures. We have been able to explain the strong temperature dependence of the spectra as an effect of the change of the internal electric field due to a temperature-dependent carrier lifetime within the framework of a simple kinetic model. By comparison with the semiclassical FK theory, the internal electric fields could be estimated. For high temperatures an exact determination of the field was possible by taking into account the spatially periodic change of the dielectric function. Starting from these values the QCFK model provided a more accurate determination of the electric field for low temperatures. By introducing a temperature-dependent subband broadening the transition from the FK model to the QCFK model could be demonstrated for our PR spectra.

*Present address: AT&T Bell Laboratories, Murray Hill, NJ 07974-0636.

[1] P.P. Ruden and G.H. Döhler, in *Proceedings of the 17th International Conference on the Physics of Semiconductors*, edited by J.D. Chadi and W.A. Harrison (Springer, New York, 1985).

[2] T.B. Simpson, C.A. Pennise, B.E. Gordon, J.E. Anthony, and T.R. AuCoin, Appl. Phys. Lett. **49**, 590 (1986).

[3] P.P. Ruden, J.A. Lehmann, N. Khan, M.K. Hibbs-Brenner, and E. Kalweit, J. Appl. Phys. **64**, 3293 (1989).

[4] X.C. Shen, H. Shen, P. Parayanthal, and F.H. Pollak, Superlatt. Microstruct. **2**, 513 (1986).

[5] M. Gal, J.S. Yuan, J.M. Viner, P.C. Taylor, and G.B. Stringfellow, Phys. Rev. B **33**, 4410 (1986).

[6] Y. Tang, B. Wang, D. Jiang, W. Zhuang, and J. Liang, Solid State Commun. **63**, 793 (1987).

[7] A.P. Thorn, P.C. Klipstein, and R.W. Glew, IEE Proc. **136**, 38 (1989).

[8] G.H. Döhler, H. Künzel, D. Olego, K. Ploog, P. Ruden, H.J. Stolz, and G. Abstreiter, Phys. Rev. Lett. **47**, 864 (1981).

[9] J.C. Maan, T. Englert, C. Uhlein, H. Künzel, K. Ploog, and A. Fischer, Solid State Commun. **47**, 383 (1983).
[10] G.H. Döhler, J.N. Miller, R.A. Street, and P.P. Ruden, Surf. Sci. **174**, 240 (1986).
[11] D.A.B. Miller, D.S. Chemla, and S. Schmitt-Rink, Phys. Rev. B **33**, 6976 (1986).
[12] D.A.B. Miller, D.S. Chemla, T.C. Damen, A.C. Gossard, and W. Wiegmann, Phys. Rev. B **32**, 1043 (1985).
[13] M. Forkel, Diploma thesis, University of Erlangen, 1990.
[14] U.D. Keil, Doctoral thesis, University of Erlangen, 1990.
[15] K.H Gulden, H. Lin, P. Kiesel, P. Riel, G.H. Döhler, and K.J. Ebeling, Phys. Rev. Lett. **66**, 373 (1991).
[16] C. Metzner (private communication).
[17] *Numerical Data and Functional Relationships in Science and Technology*, Landolt-Börnstein, New Series, Vol. 17a (Springer, Berlin, 1982).
[18] D.S. Chemla, D.A.B. Miller, P.W. Smith, A.C. Gossard, and W. Wiegmann, IEEE J. Quantum Electron. **QE-20**, 265 (1984).
[19] D.E. Aspnes and N. Bottka, in *Semiconductors and Semimetals*, edited by R.K. Willardson and A.C. Beer (Academic, New York, 1972), Vol. 9.
[20] D.E. Aspnes, in *Handbook on Semiconductors*, edited by M. Balkanski (North-Holland, Amsterdam, 1980), Vol. 2.
[21] D.E. Aspnes and A. Frova, Solid State Commun. **7**, 155 (1969).
[22] (a) B.O. Seraphin and N. Bottka, Phys. Rev. **145**, 628 (1966); (b) B.O. Seraphin, in *Semiconductors and Semimetals*, edited by R.K. Willardson and A.C. Beer (Academic, New York, 1972), Vol. 9.
[23] C. Hermann and C. Weisbuch, Phys. Rev. B **15**, 823 (1977).
[24] Y. Hamakawa and T. Nishino, in *Optical Properties of Solids: New Developments*, edited by B.O. Seraphin (North-Holland, Amsterdam, 1976).
[25] N. Linder and G.H. Döhler, Superlatt. Microstruct. **6**, 357 (1989).
[26] J. Feldmann, G. Peter, E.O. Göbel, P. Dawson, K. Moore, C. Foxon, and R.J. Elliot, Phys. Rev. Lett. **59**, 2337 (1987).
[27] K.J. Ebeling, *Integrierte Optoelektronik* (Springer, Berlin, 1989).